HHS Public Access

Author manuscript

Cell Rep Phys Sci. Author manuscript; available in PMC 2024 October 17.

Published in final edited form as:

Cell Rep Phys Sci. 2024 August 21; 5(8): . doi:10.1016/j.xcrp.2024.102120.

Enhancing RNA inhibitory activity using clamp-G-modified nucleobases

Sai Pallavi Pradeep[1], **Vikas Kumar**[1], **Shipra Malik**[1], **Frank J. Slack**[2], **Anisha Gupta**[3], **Raman Bahal**[1,4,*]

[1]Department of Pharmaceutical Sciences, University of Connecticut, Storrs, CT 06269, USA

[2]Department of Pathology, HMS Initiative for RNA Medicine, BIDMC Cancer Center, Harvard Medical School, Boston, MA 02115, USA

[3]Department of Pharmaceutical Science, University of Saint Joseph, Hartford, CT 06117, USA

[4]Lead contact

SUMMARY

We explore the potential of clamp-G nucleobase-modified peptide nucleic acids (cGPNAs) as microRNA and messenger RNA inhibitors. For proof of concept, we target miR-155, which is upregulated in diffuse large B cell lymphoma. cGPNA shows significant downregulation of miR-155 and the upregulation of its downstream targets in multiple lymphoma cell lines. Also, cGPNA treatment *in vivo* reduced tumor growth and improved survival in the U2932 cell-derived xenograft mouse model. To assess the broad application of cGPNA as an antisense modality, we also target transthyretin (*TTR*) mRNA. We establish a dose-dependent effect of antisense cGPNA on *TTR* mRNA levels. For *in vivo* studies, we conjugated cGPNA-based TTR antisense with lactobionic acid-based targeting ligand for *in vivo* liver delivery. We establish that cGPNA exhibits significant TTR protein knockdown compared to unmodified peptide nucleic acid (PNA) *in vivo*. Overall, we confirm that clamp-G-modified PNA analogs are a robust antisense therapy platform.

Graphical Abstract

*Correspondence: raman.bahal@uconn.edu.

AUTHOR CONTRIBUTIONS

R.B. conceived the study idea. S.P.P. and V.K., performed experiments. R.B., S.P.P., V.K., S.M., F.J.S., and A.G. wrote the manuscript.

SUPPLEMENTAL INFORMATION

Supplemental information can be found online at https://doi.org/10.1016/j.xcrp.2024.102120.

DECLARATION OF INTERESTS

The authors declare no competing interests.

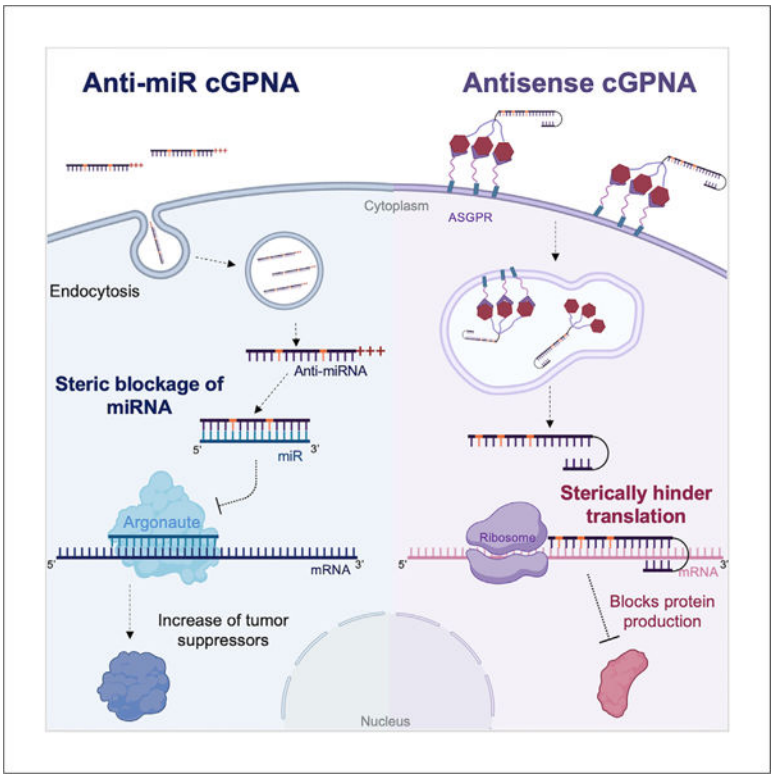

Pradeep et al. explore the use of clamp-G-modified PNAs as inhibitors of microRNA and mRNA. Clamp-G PNAs inhibit oncomiR-155 in lymphoma cell lines and improve survival in mice, and they effectively reduce TTR mRNA levels *in vitro* and *in vivo*, highlighting their potential use as a robust platform for antisense therapy.

INTRODUCTION

Peptide nucleic acid (PNA) is a synthetic nucleic acid analog that has gained attention as a therapeutic agent to target cellular RNAs and genomic DNA. PNA contains a neutral N-(2-aminoethyl)glycine backbone with attractive features, such as resistance to enzymatic degradation and non-immunogenicity after systemic delivery. PNA exhibits an antisense effect by sterically blocking the RNA translation[1] or activity. Antisense PNAs designed to target mRNA or non-coding RNAs rely on the recognition of the complementary target sites by Watson-Crick base pairing. Hence, chemical modifications have been introduced in the PNAs to increase their binding affinity and their success as therapeutics.[2] Chemically modified PNAs also exhibit superior physicochemical (such as solubility) and cellular uptake properties.[3,4] Various chemical modifications are performed on the PNA backbone or on its nucleobases. Prior work centered on modifying PNA backbones substantially improved their binding properties.[5] These are known as gamma PNAs (γPNAs). γPNAs have shown ~4°C–5°C increase in thermal melting per gamma modification in the sequence.[5,6] γPNAs have demonstrated promise as an effective tool for gene editing,[7,8] DNA targeting,[9] and microRNA (miRNA) targeting.[10,11] In contrast, nucleobase modifications onto the PNA backbone have not been tested *in vivo*.

Nucleobase modifications are aimed at introducing chemical functionalities that can either increase the base stacking interactions or form extra hydrogen bonds (H-bonds) within the complementary nucleobase.[12] Antisense oligonucleotides (ASOs) containing modified nucleobases such as 5-methy cytidine,[13,14] 2-thiothymine,[15] 5-hydroxycytosine,[15] and N6-methyl adenosine[16] have shown superior binding activity and safety profiles. However, only a few attempts have been made to modify nucleobases in the PNA.

In particular, a tricyclic cytosine base analog, 9-(2-aminoethoxy)phenoxazine (clamp-G) nucleobase modification, can potentially enhance the binding affinity of PNAs. Clamp-G exhibits improved base stacking due to its tricyclic ring structure.[17] The inclusion of clamp-G monomer in a model oligonucleotide has shown multi-fold improvement in binding affinity[17] and nuclease stability.[18] Single clamp-G substitution in a PNA oligomer increases the thermal binding (Tm) by 24°C.[19] Further, adding the guanidino group to the phenoxazine ring of the clamp-G base can augment its binding by forming five H-bonds with the guanine (Figure 1).

The clamp-G modification in PNA has been investigated for biophysical evaluations to some extent, and it has not been tested for *in vivo* biological activity. The *in vivo* applications of PNAs are limited by poor biodistribution and cellular uptake.[20,21] However, recent advancements using nanoformulations[11,22] and tissue-targeted PNA conjugates[23–25] have improved the therapeutic potential of PNAs.

Here, we report the *in vivo* application of guanidino-clamp-G-modified PNAs (cGPNAs). Following biophysical characterization, we assessed the cGPNAs' biological activity for two distinct antisense applications: inhibiting miRNA and mRNA. First, we tested the cGPNA-mediated miRNA-155 inhibition in a battery of cell lines and *in vivo* in a cell-line-derived xenograft (CDX) mouse model. Further, to broaden the scope of our work, we evaluate the antisense potential of cGPNA in targeting liver-specific *transthyretin* (*TTR*) mRNA. For *in vivo* liver-targeted delivery, we used cGPNA conjugated with di lactobionic acid (diLBA) ligand. Overall, we confirmed that the incorporation of the guanidino-clamp-G base in the PNA improved antisense efficacy against miRNA and mRNA without any adverse effects. Our findings highlight the therapeutic potential of site-specifically delivered cGPNA, which can be used for diverse antisense-based applications.

RESULTS

Design and synthesis of anti-miR-155 PNA

We designed and synthesized clamp-G containing anti-miR-155 PNAs to test in a series of lymphoma cell lines and a CDX mouse model. We designed 23-mer PNAs, both with regular and clamp-G-modified monomers, to target miR-155. Clamp-G (X) can form five H-bonds with guanine due to the expanded phenoxazine ring (Figure 1A). We designed an anti-miR-155 cGPNA with three X monomers substituted in its sequence (Figures 1A and 1B; cGPNA2). For comparison, we also synthesized a full-length regular PNA (Figure 1B; PNA1), which has been shown to inhibit miR-155 in prior studies.[10] Scramble clamp-G PNA (Figure 1B; ScR-cGPNA3) was used as a control as it was not complementary to miR-155 but contained the same nucleobase composition as cGPNA2. We added two

arginine residues at the C and N terminus of each PNA for cell permeability. PNAs were synthesized by established solid-phase synthesis-based protocols.[26] PNAs were purified by reversed-phase high-performance liquid chromatography (RP-HPLC; Figures S1A–S1C) and characterized by matrix-assisted laser desorption ionization-time of flight (MALDI-TOF; Figure S1D) mass spectrometry analysis.

In vitro binding studies of anti-miR-155

We performed gel shift assay to confirm the binding affinity of PNAs with a miR-155 target (DNA-155). Indicated concentrations of PNA1 and cGPNA2 were incubated with the miR-155 target in physiological buffer and temperature (37°C) conditions overnight (Figure 1C). We performed the binding studies using polyacrylamide gel electrophoresis (PAGE) followed by SYBR Gold staining. We noted an increase in the intensity of the retarded miR-155-PNA band in a dose-dependent manner. We observed the disappearance of the unbound miR-155 at a miR-155: PNA1 stoichiometric ratio of 1:1 (Figure 1C). Although cGPNA2 showed complete binding at a lower concentration (Figure 1C, lane 5). We also measured the bound and unbound fractions for all the PNAs (Figure 1D). At 0.8 μM concentration, cGPNA2 was 98% bound while PNA1 was ~50% bound, indicating the superior binding affinity of cGPNA2 over PNA1 to the target. This superior binding in the cGPNA2 could be due to the additional H-bonds and base-stacking interactions formed by clamp-G monomers.

Antisense activity of clamp-G PNA in lymphoma cells

Diffused large B cell lymphoma (DLBCL) is an aggressive non-Hodgkin lymphoma, and miR-155 has been identified as a key player in its development and progression.[27] miR-155 was significantly upregulated in plasma samples from DLBCL patients. Inhibition of miR-155 in B cell lymphoma cell lines has been shown to reduce their proliferation.[28] Hence, we evaluated the antisense activity of clamp-G PNA in multiple DLBCL cell lines (U2932 and SUDHL-5). Using gene expression analysis, we quantified the levels miR-155 and its downstream targets after treatment with PNAs. U2932 and SUDHL-5 cells were treated with 4 μM PNA1 and cGPNA2 for 48 h. Our gene expression (RT-PCR) results in U2932 cells confirmed 62% and 72% inhibition of miR-155 with PNA1 and cGPNA2 treatments, respectively, relative to the PBS-treated groups. Similarly, we noted PNA1 and cGPNA2 treatments resulted in 87% and 91% downregulation of miR-155, respectively, in the SUDHL5-treated cells (Figure 2A).

We further evaluated the gene expression of validated downstream tumor suppressor targets, *Suppressor of cytokine signaling* (*SOCS1*), *Forkhead box O3* (*FOXO3A*), and *Colony-stimulating factor-1 receptor* (*CSF1R*).[29] *SOCS1* enhances the phosphorylation of p53, thereby increasing its binding to p53 target genes and inhibiting cell proliferation.[30] We observed a 2.5-fold increase in SOCS1 levels in cGPNA2 treated U2932 cells compared to PNA1 (Figure 2B). Similarly, cGPNA2 treatment showed a 2.4-fold increase in *SOCS1* mRNA in SUDHL-5 cells (Figure 2C). *FOXO3A* is a transcription factor that controls apoptosis-related genes, and its dysregulation by miR-155 contributes to tumorigenesis.[31] We observed a ~3- and 1.8-fold increase in *FOXO3A* levels after treatment with cGPNA2 in U2932 and SUDHL-5, respectively (Figures 2B and 2C). We also found that treatment

with cGPNA2 led to a 2.8- and 7.9-fold increase in *CSF1R* levels in U2932 and SUDHL-5, respectively (Figures 2B and 2C). These cell-culture-based results suggest that cGPNA2 possesses superior miR-155 inhibitory activity compared to the PNA1.

We also evaluated the gene expression of miR-155-associated indirect downstream oncogenes. Prior studies established that upregulation of miR-155 increases the *myeloid cell leukemia-1* (*MCL1*),[32] *c-Myc*,[33] and *B cell lymphoma 2 (BCL2)*[34] gene expression. We observed 10% and 30% downregulation of *MCL1* in U2932 cells treated with PNA1 and cGPNA2, respectively. Similarly, cGPNA2 treatment resulted in 40% downregulation of *MCL1* in SUDHL-5 cells (Figure 2D). In 21%–44% of DLBCL patients, *c-Myc* and *BCL2* are translocated, causing dysregulated expression and driving carcinogenesis.[35] We observed a 25% and 30% reduction in *c-Myc* expression in U2932 cells treated with PNA1 and cGPNA2, respectively. We also observed a 30% reduction in *BCL2* gene expression in U2932 cells treated with cGPNA2 (Figure S2A). SUDHL-5 cells treated with cGPNA2 also result in a significant repression of *c-Myc* (78%) and *BCL2* (87%) gene expression levels (Figure S2B). By western blot analysis, we confirmed the anti-miR effect of cGPNA2 on the validated miR-155 downstream target, MCL1. We noted a ~50% lower levels of MCL1 in cGPNA2-treated U2932 (Figure 2E) and SUDHL-5 (Figure 2F) cells relative to the PBS control.

Different doses of PNA1 and cGPNA2 were tested using trypan blue assay and CytoTox assay to determine the effect on the viability of lymphoma cells. In U2932 and SUDHL-5 cells, cGPNA2 treatment results in a dose-dependent reduction in cell viability. Overall, using trypan blue assay, we noted a ≥60% reduction in U2932 and SUDHL-5 cell viability at a 4 μM dose of cGPNA2. PNA1 exhibited a 30% and 40% decrease in viability of U2932 and SUDHL-5 cells, respectively (Figures 2G and 2H). We also estimated the luminescence from dead cells using CytoTox assay. U2932 and SUDHL-5 cells treated with cGPNA2 and PNA1 showed a dose-dependent increase in the dead cells after 48 h of treatment (Figures S2C and S2D). Further, we performed the annexin V apoptosis assay after a 4 μM treatment of cGPNA2 and PNA1. After cGPNA2 treatment, we observed a ~20% increase in the late apoptotic population ($7AAD^+$ and annexin V^+), significantly higher than PNA1(~10%) and PBS control (Figure S2E). Our results indicate that cGPNA2 can efficiently downregulate miR-155 in the lymphoma cell lines with subsequent effect on decreasing its cell viability.

Antisense activity of clamp-G PNA in U2932 CDX mouse model

We evaluated the efficacy of cGPNA2 *in vivo* in a U2932 CDX mouse model. We conducted a short-term efficacy study wherein we administered a single dose of PNA1, cGPNA2, and Scr-cGPNA3 by intratumoral (i.t.) route (Figure S3A). After 48 h, we evaluated miR-155 knockdown and impact on downstream targets via gene expression and western blot analysis. We observed a 50% reduction in miR-155 with PNA1 and cGPNA2 treatments compared to Scr-cGPNA3 (Figure 3A). cGPNA2 treatment also resulted in the upregulation of miR-155 downstream targets (*FOXO3A*, *WEE1*, *SOCS1*, and *CSF1R)* compared to the Scr-cGPNA3. However, PNA1 did not exhibit an upregulation in downstream targets in comparison to the Scr-cGPNA3-treated cells (Figure 3B). We confirmed the effect of cGPNA2 on the validated downstream targets *FOXO3A*[33] and *WEE1*[36] by western

blot analysis. Treatment with cGPNA2 significantly upregulated WEE1 (Figure S3B) and FOXO3a (Figure S3C) in comparison to ScR-cGPNA3. Gene expression and western blot analysis showed an 80% (Figure 3C) and 10% (Figure 3D) decrease in *MCL1* mRNA and protein levels after treatment with cGPNA2.

We conducted a survival study to determine the pre-clinical efficacy of clamp-G PNAs in the U2932 CDX model. U2932 xenograft tumors of about 100–150 mm^3 were treated with three doses of PNA1, cGPNA2, and Scr-cGPNA3 i.t. (Figure S3D). The study employed a tumor volume of 2,000 mm^3 as the endpoint for survival analysis. Mice treated with cGPNA2 had a median survival of 21 days compared to Scr-cGPNA3, which survived 15 days (Figure 3E). In contrast, the median survival of PNA (16 days) was not significantly different from the ScR-cGPNA3-treated group (Figure 3E). We performed an immunohistochemical analysis of Ki67, a proliferation maker, on the tumors collected at the end of the survival study. We observed a 40% reduction in Ki67 staining in the cGPNA2 treatment group compared to PNA-1 and Scr-cGPNA3 (Figures 3F and 3G).

To test the safety of PNA treatment, we performed histopathological analysis of major organs (Figure S4A), complete blood count (Figure S4B), and organ weight (Figure S4C) in all treatment groups. Our findings suggest that cGPNA2 efficiently reduced miR-155 levels and increased its downstream targets, contributing to its anti-tumor activity without inducing adverse effects.

Evaluation of clamp-G PNA in silencing transthyretin

To ensure the broad application of clamp-G-modified nucleobases, in a proof-of-concept study, we tested the clamp-G PNAs antisense activity in targeting transthyretin (TTR) mRNA. The US Food and Drug Administration (FDA) has approved ASOs and small interfering RNAs (siRNAs) for treating hereditary transthyretin-related amyloidosis (hTTR). hTTR is a genetic autosomal dominant inherited disorder. Point mutations in the TTR gene lead to misfolded protein aggregation and deposition.[37] Hence, ASO and gene-editing therapies are effective.[38] We explored the potential application of clamp-G PNA as an antisense to inhibit TTR. The clamp-G PNAs target the mRNA in exon 1, 64 base pairs after the translation start site. We assessed clamp-G PNA ability to inhibit mRNA translation and reduce TTR proteins *in vitro* and *in vivo*. We designed and synthesized tail-clamp PNAs with and without the clamp-G modification that can target wild-type TTR protein as proof of concept. Tail-clamp PNAs were used as they can bind to the target mRNA via Watson-Crick and Hoogsteen base pairing to form a highly stable clamp and inhibit the progression of translation machinery.[39] Since the clamp region binds via Hoogsteen base pairing, we introduced a modification of two clamp-G nucleobases in the tail region that does not overlap with the clamp region binding of the PNA. TTR-specific PNAs (PNA4 and cGPNA5) and a scramble PNA6 were synthesized and characterized as previously described (Figure 4A). ScR-PNA6 was used as a control as it was not complementary to *TTR* mRNA but contained the same nucleobase composition as cGPNA5. For delivery of PNAs across the cellular membrane in hepatocytes, diLBA was conjugated on the N terminus of PNAs (Figure 4A; PNA4-L, cGPNA5-L, and ScR-PNA6-L) using succinic acid as a molecular handle (Figure S5A). Recently, we established that diLBA-based ligands can selectively

target the liver post systemic delivery. Conjugates were purified by RP-HPLC (Figures S5B–S5D) and characterized by MALDI-TOF (Figure S5E) mass spectrometry analysis.

We used PAGE assay to evaluate the binding affinity of PNA4, cGPNA5, and ScR-PNA6 with the *TTR* mRNA target. We incubated PNAs at indicated concentrations with the TTR target in physiological buffer and temperature (37°C) conditions overnight (Figure 4B). We observed an increase in the intensity of the retarded complex (PNA-TTR) with the increase in PNA4 and cGPNA5 concentrations. As expected, we did not notice any binding for TTR mRNA incubated with the Scr-PNA6. Prior work has established that the conjugation of the ligand to the PNA does not impact its target recognition.[23] Hence, we did not perform the PAGE assay for PNA4-L and PNA5-L.

We evaluated the translation inhibition efficiency of TTR PNAs using rabbit reticulocyte lysate (RRL). We first synthesized *TTR* mRNA via *in vitro* transcription, treated it with DNase, and purified it. Purified mRNA was incubated with different concentrations of PNA4, cGPNA5, and ScR-PNA6 for 3 h at 37°C. Following this, the TTR mRNA:PNA complexes were incubated in RRL, followed by western blot analysis (Figure 4C). We noted a significant reduction (62%) of TTR protein when *TTR* mRNA was incubated with cGPNA5 at a 1:4 stoichiometric ratio relative to control (Figure 4D). While PNA4 caused a 5% decrease in TTR protein levels at a 1:4 stoichiometric ratio, cGPNA5 treatment resulted in a much larger reduction at 62%. ScR-PNA6 showed no reduction in TTR protein at a 1:2 and 1:4 stoichiometric ratios. These results confirm that cGPNA5 has a better antisense effect than PNA4 and ScR-PNA6.

Next, we evaluated the *TTR* mRNA knockdown in HepG2 cells. We treated HepG2 cells at different doses (1, 2, and 4 μM) for 24 h with PNA4, PNA4-L, cGPNA5, and cGPNA5-L and compared them with ScR-PNA6 (Figures 4E and 4F). Using gene expression analysis, we quantified the *TTR* mRNA levels. For PNA4-L, we observed a dose-dependent reduction in *TTR* mRNA levels that was ≥60% at 1, 2, and 4 μM doses in comparison to ScR-PNA6 (Figure 4E). PNA4 exhibited no significant reduction in *TTR* levels in comparison to ScR-PNA6 (Figure 4E). This could be due to the reduced uptake in HepG2 cells. We noted a dose-dependent reduction in *TTR* mRNA in the HepG2 cells treated with cGPNA5 and cGPNA5-L (Figure 4F). At 4 μM dose, we observed a 69% reduction in cGPNA5 and 90% reduction in cGPNA5-L. The significantly lower (≥85%) knockdown of *TTR* mRNA at 2 and 4 μM doses with cGPNA5-L can be attributed to its efficient uptake in HepG2 cells. To establish that PNAs sterically block TTR mRNA and do not degrade, we performed the RT-PCR with primers binding to the 3′ UTR and observed no change in TTR levels (Figure S6).

In vivo evaluation of clamp-G PNA-mediated transthyretin knockdown

We conducted a short-term study to evaluate the TTR knockdown in C57BL/6 mice. We subcutaneously administered cGPNA5, cGPNA5-L, and ScR-cGPNA6 at 5 mg/kg on alternate days (Figure 5A). The dose regimen of PNA was according to the prior efficacy of the PNA-L conjugate in the wild-type mice.[23] After 48 h of the second dose, we evaluated the *TTR* mRNA knockdown in the liver via gene expression. We observed a 50% reduction in *TTR* mRNA with cGPNA5-L compared to ScR-PNA6 and cGPNA5 (Figure 5B). We

collected plasma from mice before and after the study and compared the fold change in the TTR protein levels by enzyme-linked immunosorbent assay (ELISA). We observed a 30% reduction in TTR protein levels for cGPNA5-L compared to ScR-PNA6 after treatment (Figure 5C). We were able to observe significant TTR knockdown in the plasma of C56BL/6 mice using the clamp-G PNA.

DISCUSSION

In this report, we established that clamp-G PNAs are a potential anti-miR and antisense for *in vivo* application. In prior work, backbone modifications introduced functional groups in the PNA's alpha, beta, and gamma positions. PNAs containing arginine or lysine residues at the alpha position (αPNA) showed improved PNA:DNA duplex stability in a stereochemical manner.[40,41] The introduction of a methyl group at the β-position (βPNA) has shown comparable stability to unmodified PNA. While circular dichroism spectra of βPNA indicated helical pre-organization, this secondary structure did not improve the binding due to unfavorable steric interactions arising from β-methyl groups.[42] The γ-backbone modification (γPNA) has a high binding affinity to the target due to its pre-organization helical conformation[5] and has been explored extensively for its antisense[43] and antigene applications.[9] Although backbone modifications show improvement in binding affinity and thermal melting, they are influenced by the chirality and steric properties of the substituted group. Nucleobase modifications such as clamp-G are not influenced by these properties, and adding one nucleobase modification can achieve up to a 24°C increase in thermal melting temperature. In addition, clamp-G can increase duplex stability as they have increased π – π stacking interaction.[19] Despite these advantages, the application of cGPNAs remains limited due to high cost as it requires a multi-step synthesis process and low reaction yields (5%–10%).[44] *In vitro*, clamp-G nucleobase has been evaluated with phosphorothioate backbone to target the $p27^{kip1}$ (cyclin-dependent kinase inhibitor). However, *in vivo* evaluation has not been pursued.[45] Prior work has investigated the biophysical properties of cGPNA to invade double-stranded DNA in a sequence-dependent manner.[46,47] These studies suggest the potential of cGPNAs to invade and inhibit dsDNA, but further *in vitro* and *in vivo* studies are necessary to broaden its application.

Cytosine analogs such as 6-phenylpyrrolocytosine (PhpC) have been used in antisense oligonucleotides such as siRNA,[48] locked nucleic acids, and PNA.[49] PhpC is a fluorescent cytosine analog modified to introduce a guanidium group. This meta-substituted PhpC can form five H-bonds with guanine, which increases the Tm by 12°C per nucleobase addition. However, meta-substituted PhpCs have not been evaluated for antisense applications.[50] Other cytosine analogs, including 2-aminopyridine, 4-thiopseudoisocytosine, and pseudoisocytosine, show stabilized Hoogsteen base pairing in triplex PNAs.[51] These modifications in tail-clamp PNA designs were evaluated for *in vivo* and *in vitro* efficacy. Our study established the application of regular and tail-clamp PNAs with clamp-G substitutions.

To our knowledge, this is the first study that explores the use of cGPNAs for antisense applications *in vivo*. We have compared the efficacy of cGPNAs with unmodified PNAs for their efficiency at inhibiting miRNA and mRNA. PNAs have been explored as miRNA antagonists, targeting miR-21,[52,11] miR-210,[22] miR-155,[10,25,53] miR-10b,[11] miR-33,[54,55]

miR-141-3p,[56] miR-122,[57] miR-145, and miR-101[58] in cancer, fibrosis, and metabolic disorders. Among oncomiRs, miR-155 is an important molecular target in lymphomas. Drug candidates targeting miR-155, such as coba-mersen, have shown promise in reducing tumor burden in cutaneous T cells lymphoma.[28] Furthermore, various γPNA designs, such as tail-clamp and anti-seed PNAs, have been efficacious at inhibiting miR-155[10,53]. Here, we explored the anti-miR activity of clamp-G-modified PNA and observed ~80% reduction in miR-155 levels, which is comparable to the 80% knockdown achieved with tail-clamp γPNA in our earlier work.[10] Interestingly, while both cGPNA and regular PNA showed knockdown of miR-155, cGPNA showed significantly higher upregulation of tumor suppressor proteins. This can be attributed to the enhanced binding affinity of cGPNAs with the target sites. We also showed that cGPNAs are safe and improve survival in a mouse model compared to the regular PNAs. Unmodified PNAs have limited cellular uptake. Prior work has established that using octaarginine peptides increases the cellular uptake of PNAs in cells.[59,60] High cationic charge density can disrupt lysosomes, producing reactive oxygen species (ROS). These ROS can damage the plasma membrane and reduce cell viability.[61,62] We established that four arginine increase PNA cellular uptake with no cellular toxicity.[53] Hence, in our anti-miR evaluation of cGPNAs, we conjugated four arginines to their termini to improve cellular transfection.

PNAs have also been explored for targeting mRNAs, and, unlike other antisense oligonucleotides, their effect is not RNase H1 dependent. The PNAs we designed can target both wild-type and mutated versions of TTR as all pathogenic mutations exist on exons 2, 3, and 4.[63,64] PNAs bind to mRNA and inhibit translation by a steric hindrance-based mechanism. In a previous study, single-stranded γPNAs have effectively reduced *β-catenin* mRNA by ~30%.[65] We explored a tail-clamp PNA design with nucleobase modifications to achieve an effective mRNA knockdown. We tested our hypothesis by targeting *TTR* mRNA translation mutated in hTTR. Treatment with optimized cGPNA-L resulted in an 80% reduction in *TTR* mRNA levels. FDA-approved therapies for hTTR use N-acetyl galactosamine (GalNAc)-conjugated siRNA to target the liver selectively. Our study used LBA as it has comparable liver-targeted delivery to GalNAc.[23] Divalent LBA is covalently conjugated to the PNA and allows for the cellular uptake by the asialoglycoprotein receptor present in HepG2 cells and hepatocytes.[23] We used a tail-clamp cGPNA treatment at 5 mg/kg and achieved a 30% knockdown of TTR protein, lower than the 60% achieved by siRNA at 2.5 mg/kg.[66] This can be attributed to the mechanism of siRNA-mediated mRNA silencing, which is different from the steric blockage mechanism of PNA. siRNA associates with the argonaute proteins to form the RNA-induced silencing complex (RISC) and cleaves the target mRNA, after which the activated complex can be recycled.[67,68] Endosomal entrapment of antisense drugs can also limit the amount of drug available for silencing and needs to be investigated in the context of clamp-G PNAs. Further, the dose range and frequency of dosing need to be optimized and evaluated in transgenic disease mice (hTTR V30M HSF1$^{\pm}$). hTTR V30M HSF1$^{\pm}$ mice were used in the pre-clinical evaluation of siRNA-mediated silencing (Partisiran) of TTR and subsequently approved by the FDA.[69] The hTTR V30M HSF1$^{\pm}$ transgenic mice model contains the human V30M mutation and is heterozygous for heat shock transcription factor (HSF1), which causes TTR deposition in tissues.[70] It would be interesting to evaluate cGPNA-based antisense in a diseased mouse

model and examine the TTR mRNA knockdown and its subsequent effect on reduced protein deposition and improved disease phenotype.

The targeted delivery-based strategies to disease organs can minimize the off-target effects. In our prior work, based on Basic Local Alignment Search Tool (BLAST) and RNA sequencing (RNA-seq) analysis, we established that short anti-seed anti-miRs in conjunction with the central nervous system (CNS)-targeted nanoformulations minimize the off-target effects and target miR-21 and miR-10b for brain cancer therapy.[11] Hence, the targeted delivery of RNA-targeted strategies can potentially mitigate the off-target effects in a clinical setting.[55,71–73] Our study is centered on developing and testing the biological activity of full-length chemically modified cGPNA-based PNAs in cell culture and *in vivo*. Although miR-155 and TTR are well-established clinical targets,[27,28,38,74] prior studies indicated these targets do not illicit the off-target effects.[28,75,76] We also performed BLAST analysis on the PNAs targeting TTR and miR-155. We only identified four genes as potential off-target sites for TTR PNAs with high E values. From BLAST sequencing analysis, it is established that a higher E value indicates a high probability of chance or false hits.[77] From bioinformatic coverage analysis of the genome, we expect that the full length of cGPNA (20 mer) will bind to perfect match binding targets only by Watson-Crick base pairing.[78] Although we do not anticipate any adverse events due to non-specific binding of cGPNA, for the sake of thoroughness, whole-genome sequencing-based methods are still required in future work to rule out the absolute possibility of off-target effects inclusively.

Various delivery strategies for cell-penetrating peptides, nanoparticles, and liposomes have been tested to improve their transfection efficiency.[79] Tumor-targeted delivery of cGPNA can be achieved by conjugating it to pH-low insertion peptides (pHLIPs). Another potential delivery strategy could be an encapsulation of cGPNA in nanoparticles composed of poly (lactide-co-glycolic acid) (PLGA), PLGA/poly-L-histidine,[80] or bioadhesive aldehyde functionalized poly (lactic acid)-hyperbranched polyglycerol nanoparticles[81] We utilized a ligand-targeted delivery and observed a significant reduction in *TTR* mRNA levels when HepG2 cells were treated with PNA4-L and PNA5-L. PNA4, which was not conjugated to the ligand, showed no knockdown. Interestingly, cGPNA5 showed a dose-dependent knockdown of *TTR*, suggesting that clamp-G influences the uptake of PNAs.

Overall, we demonstrated that the integration of clamp-G nucleobase can effectively increase the RNA-inhibitory activity of PNA-based strategies. These advances promise to extend the application of cGPNA and various other nucleic acid classes for improved antisense and antigene applications.

EXPERIMENTAL PROCEDURES

Resource availability

Lead contact—Further information and requests for resources and reagents should be directed to and will be fulfilled by the lead contact, Raman Bahal (raman.bahal@uconn.edu).

Materials availability—This study did not generate new unique reagents.

Data and code availability—This paper does not report original code.

Materials and methods

Fmoc-protected clamp-G monomer and Boc-protected PNA monomers and were purchased from ASM Research Chemical, Germany. The 4-methylbenzhydrlamine (MBHA) resin, amide coupling reagents, and Boc-MiniPEG3 were purchased from Vivitide. Fmoc-lys(Boc)-OH, mono-*tert*-butyl succinate, LBA was purchased from Sigma-Aldrich. U2932, SUDHl-5, and HepG2 cell lines were purchased from American Type Culture Collection (ATCC). Eagle's minimum essential medium (EMEM), RPMI-1640 medium, trypsin-EDTA, penicillin-streptomycin, and fetal bovine serum (FBS) were purchased from ATCC.

Synthesis of PNA oligomers

PNAs were synthesized on MBHA resin using Boc and Fmoc chemistry and standard solid-phase synthesis protocols.[26] PNAs were synthesized from the C to-N terminus (3′ to 5′) direction The anti-miR PNAs had two arginine residues conjugated to the N and C terminus. The TTR PNAs with ligands were capped with succinic acid at the 5′ end through a trioxo-miniPEG spacer to generate –COOH in the PNA structure. PNAs were cleaved from the resin in trifluoracetic acid (TFA): trifluoromethane sulfonic acid:m-cresol:thioanisole at a ratio of 6:2:1:1 (v/v). Diethyl ether was used to precipitate the cleaved PNA followed by washing and vacuum drying. Crude PNAs were purified using Shimadzu RP-HPLC over a C18 semi-preparative column with gradient elution using water and ACN (containing 0.1% TFA). The identity of the PNAs was confirmed by MALDI-TOF and concentration was determined by measuring absorbance at 260 nm via UV-visible (UV-vis) spectrometry. The extinction coefficient of individual monomers used for calculating PNA concentration (6,600 $M^{-1}cm^{-1}$ [C], 13,700 $M^{-1}cm^{-1}$ [A], 8,600 $M^{-1}cm^{-1}$ [T], 11,700 $M^{-1}cm^{-1}$ [G], 11,396 $M^{-1}cm^{-1}$ [X]). TTR PNAs (PNA4, cGPNA5, and ScR-PNA6) were conjugated with diLBA ligand in a solution-phase amide coupling reaction as described previously.[23] Briefly, 100 nmol of PNA (1 equiv) in DMSO (100 μL) was mixed with N,N-diisopropylethylamine (DIEA, 5 equiv) and acetylated diLBA ligand ($diLBA_{Ac,}$ 5 equiv). After 5 min of shaking at room temperature (RT), amide coupling reagent hexafluorophosphate azabenzotriazole tetramethyl uronium (HATU, 3 equiv) was added to the reaction. After 4 h of reaction, PNA conjugates (PNA-$diLBA_{Ac}$) were purified using RP-HPLC and subjected to deacetylation using a catalytical amount of sodium methoxide (NaOMe) in methanol. The resulting PNA-diLBA conjugates were purified on RP-HPLC. For quality control of PNA conjugates, MALDI-TOF and HPLC purity profiles were performed.[23]

Gel shift assays

The binding affinity of PNAs with the target was determined as previous described.[10] In brief, PNAs were incubated with target miR-155 or TTR (1 μM) at different ratios in buffer mimicking physiological conditions (2 mmol/L $MgCl_2$, 150 mmol/L KCl, 10 mmol/L NaPi). The samples were incubated at 37°C for 16 h and run on a 10% polyacrylamide gel at 120 V for 40 min. The gel was stained with SYBR Gold for 2 min and visualized using Gel Doc EZ Imager (Bio-Rad).

Cell culture

U2932 and SUDHL-5 cells were cultured in RPMI medium and HepG2 cells were cultured in EMEM medium. Media were supplemented with 10% FBS and 1% Pen-Strep and cells were maintained at 37°C and 5% CO_2.

Gene expression by RT-PCR

For the anti-miR experiments, 400,000 U2932 or SUDHL-5 cells were seeded in a 12-well plate. The cells were treated with 4 μM PNA, cGPNA2, or PBS and incubated for 48 h. For the antisense experiments, 200,000 HepG2 cells were seeded in a 12-well plate. Cells were treated with different doses (1, 2, and 4 μM) of PNA4, PNA4-L, PNA5, and PNA5-L and incubated for 24 h.

The total RNA from the cells was extracted using the RNeasy Mini Kit (Qiagen). cDNA was synthesized using high-capacity cDNA reverse transcription following the recommended cycling conditions. Random primers were used for downstream targets and miR-155 (Hs01374569_m1) and U6-specific primers (Hs00211890_m1) were used for microRNA cDNA preparation. Taqman gene expression assays for *MCL-1* (Hs06626047_m1), *SOCS1*(Hs00705164_m1), *FOXO3A* (Hs00818121_m1), *CSF1R* (Hs00911250_m1), *c-Myc* (Hs00153408_m1), *Bcl-2* (Hs00608023_m1), *Bcl6* (Hs00277037_m1), and *TTR* (Hs07288491_m1, Mm01158182_m1; Thermo Fisher Scientific) were used to amplify the respective mRNAs using the specified cycling conditions in the QuantStudio 5 real-time PCR detection system (Thermo Fisher Scientific, USA). *GAPDH* was used as the reference gene and fold change in mRNA expression was obtained by normalizing against the untreated cells.

Cell viability

For the trypan blue Assay, U2932 and SUDHL-5 were seeded in 96-well plates at a density of 10,000 cells/well. The cells were treated with different concentrations (0.5, 1, 2, and 4 μM) of PNA1 and cGPNA2. After 48 h of incubation, cell viability was measured using trypan blue staining and counted on an automated cell counter (Bio-Rad, USA).

For the CytoTox-Glo assay, U2932 and SUDHL-5 were seeded in 96-well plates at a density of 10,000 cells/well. The cells were treated with different concentrations (0.5, 1, 2, and 4 μM) of PNA1 and cGPNA2. After 48 h of incubation, CytoTox-Glo reagent was added according to the manufacturer's instructions (Promega, #G9290). Luminescence from dead cells was measured on an infinite 200 PRO microplate reader (TECAN).

Apoptosis assay

Apoptosis was assessed using the fluorescein isothiocyanate (FITC) annexin V apoptosis detection kit (BD Pharmingen), and 200,000 U2932 cells were seeded in a 12-well plate. The cells were treated with 4 μM PNA1 and cGPNA2 or PBS (control) and incubated for 48 h. The cells were washed with cold PBS twice and cell pellets were suspended in Ix annexin V-binding buffer. The cells were then counted and stained with phycoerythrin (PE) annexin dye and 7-amino-actinomycin (7AAD) as per the manufacturer's instructions. Cells were acquired using LSR Fortessa X-20 Cell analyzer and data were processed using FlowJo.

Cells that stain positive for both FITC annexin V and phosphatidylinositol (PI) are identified as a late stage of apoptosis or are undergoing necrosis. Cells that stain negative for both dyes are identified as alive.

Western blot

For western blot, 400,000 U2932 and SUDHL-5 cells were seeded in a 12-well plate and treated with 4 μM PNA1 and cGPNA2 for 48 h. Total protein was extracted from cell pellets, enriched human tumor cells, using 1× RIPA buffer (Cell Signaling Technology, #9806) containing protease inhibitor. The concentration of protein was determined using an absorbance-based DC protein assay (Bio-Rad, USA). Equal amounts of protein (25–40 μg) were separated on a 4%–20% SDS-PAGE gel followed by transfer to the polyvinylidene fluoride (PVDF) membrane. MCL-1 (CST, #5453), FOXO3a (CST, #2497), and WEE1 (CST, #13084) proteins were probed using rabbit monoclonal primary antibody in 3% BSA at 4°C overnight. Cyclophilin B (CST, #43603) and GAPDH (CST, #4970) were probed as the endogenous controls. The bands were detected using anti-rabbit immunoglobulin (Ig) G HRP linked secondary antibody (Cell Signaling Technology, #7074) (1:2,000 dilution, 5% milk in Tris-buffered saline containing 0.1% Tween 20) and horseradish peroxidase (HRP) substrate (Millipore sigma, USA). The blots were imaged using ChemiDoc imager (Bio-Rad, USA) and band intensities were quantified using ImageJ 1.52a and cyclophilin B or GAPDH as a loading control.

Study approval

All animal experiments were performed at the University of Connecticut, Storrs in compliance with and approved by the Institutional Animal Care and Use Committee (IACUC). The authorization number for approved IACUC is A21-041.

In vivo studies

The short-term efficacy and survival study used female NOD scid gamma (NSG) mice (NOD.Cg-Prkdcscid Il2rgtmWjl/SzJ, strain 005557) weighing 20–23g were procured from the Jackson Laboratory. For this, 1×10^7 U2932 cells were suspended in RPMI-1640 medium and subcutaneously injected in the right flank of 6-week-old NSG mice. The tumor size was monitored.

Short-term efficacy—The mice were treated when the tumors reached a volume of ~300 mm^3 for U2932 xenografts. γPNA2-NLS was administered via the i.t. route at 5 mg/kg in U2932 xenograft mice for 48 h. Tumors were dissociated using the protocol detailed below and cells were used for gene expression and western blot analysis.

Survival study—Mice bearing tumors about 100–150 mm^3 were divided into four groups. Mice were treated with either saline, PNA1, cGPNA2, or Scr-cGPNA3 ($n = 6$). PNAs were administered at 1 mg/kg dose on days 1 and dose of 2 mg/kg on days 7 and 14. The change in tumor volume and body weight was measured every day. Mice were euthanized when the tumor volume reached 2,000 mm^3. Blood was collected via cardiac puncture in 1.5-mL tubes containing 0.5 M EDTA. Organs including tumor, liver, kidney, spleen, heart, and lung were collected and weighed. Tumor fractions and all organs were kept in 10% formalin and

submitted for histology. The complete blood count (CBC) analysis was performed on the collected blood samples using Sysmex CBC analyzer (USA).

Tumor dissociation—The collected tumor fragments from short-term study and survival study were processed to enrich the implanted human tumor cells. The tumor fragments were chopped into small fragments under sterile conditions and dissociated using dispase (Stemcell Technologies, #100–0396), collagenase (Worthington, #LS004194), and RPMI medium at 37°C for 1.5 h. The dissociated tumor fragments were centrifuged, washed with PBS, and passed through a 70-μm filter. The collected single-cell suspension of tumor cells was centrifuged and incubated with 1 mL of trypsin for 5 min at RT. Cells were then diluted in RPMI medium and passed through a 40-μm filter. The collected cells were centrifuged and resuspended in 0.5–0.7 mL of red blood cell (RBC) lysis buffer at RT for 4 min. Cells were then diluted in PBS and centrifuged. The obtained tumor cell pellet was suspended in 0.5% BSA and cell count was determined. To enrich the human tumor cells, 2×10^7 live cells were incubated with 20 μL of mouse cell depletion cocktail (Miltenyi Biotec, #130-104-694) at 4°C in dark for 15 min. Cell suspension was then diluted to 0.5 mL using 0.5% BSA and passed through the LS column (Miltenyi Biotec, #130-042-401). The collected cells were the enriched human tumor cells. Cells were centrifuged and pellets were stored at −80°C for further analyses.

TTR knockdown evaluation—C57BL/6J mice (stock 000664) were procured from Jackson Laboratory when they were 7–10 weeks old and housed in a pathogen-free environment with standard food and water. Blood was collected retro-orbitally, and plasma was separated (3,000 rpm for 15 min) and used for TTR analysis by ELISA. cGPNA5, cGPNA5-L, and ScR-cGPNA6-L were administered subcutaneously with a dose of 5 mg/kg on day 1 and 3. Mice were evaluated for body-weight changes and visual signs of toxicity during the treatment. On day 5, mice were euthanized and blood was collected by using cardiac puncture, and plasma was separated and used for TTR analysis by ELISA. Major organs, including liver, lungs, heart, kidney, and spleen, were harvested in PBS thoroughly soaked on absorbent pads and weighed. A portion of the liver was snap-frozen using dry ice and stored at −80°C for RNA extraction.

In vitro transcription and translation

We maintained an RNase-free environment. All reagents were RNase free and we used dedicated RNase-free pipettes with filter tips. The *in vitro* transcription (IVT) template used was TTR plasmid (pLDNT7_nFLAG), purchased from DNASU plasmid repository. The plasmid template contained a T7 promoter and TTR target sequence. The plasmid was linearized using fast digest PteI (Thermo Fisher Scientific, #FD2134) restriction enzyme. RNA was produced following the protocol of the HiScribe T7 high-yield mRNA Kit (New England Biolabs, USA, #E2040S). The IVT reaction was then carried out according to the standard protocol, except that uridine-5'-triphosphate (UTP) was replaced by pseudo-UTP, respectively. We used co-transcriptional capping with anti-reverse cap analog (New England Biolabs, S1411L). Finally, mRNA purification was achieved by RNeasy Mini Kit (Qiagen, #74106) according to the manufacturer's instructions. mRNA was quantified using Quant-it RiboGreen RNA Assay Kit (Invitrogen, #R11491). The mRNA was incubated

with different ratios of PNA4, cGPNA5, and ScR-cGPNA6 at 37°C for 3 h. Purity and TTR mRNA and PNA mixtures were incubated in RRL (Promega, #L4960) to quantify the translation inhibition of the PNAs using the manufacturer's instructions. After incubation for the indicated time, equal aliquots of the reaction mixture were subjected to SDS-PAGE. The SDS-PAGE-separated proteins were transferred onto a PVDF membrane. TTR (CST, #29872) protein was probed using rabbit monoclonal primary antibody in 3% BSA at 4°C overnight. The proteins were probed as described in the ''western blot'' section.

ELISA

To measure TTR levels in mouse serum, we used ELISA kits. Serum was collected at the indicated time and subjected to ELISA using commercial kits from Abcam (ab282297) following the manufacturer's instructions. All samples were run in duplicate in dilutions recommended by the manufacturer. Absorbance was determined at 450 nm using an iMark Bio-Rad microplate absorbance reader.

Statistical analysis

GraphPad Prism 9 (version 9.4.1) was used for statistical analysis. The data were reported as mean ± SEM and the number of replicates is included in the figure captions. An unpaired two-tailed t test was performed for experiments to test significance between the two groups. Two-way ANOVA was performed to test statistically significant differences between multiple groups. A p value less than 0.05 was considered statistically significant.

Supplementary Material

Refer to Web version on PubMed Central for supplementary material.

ACKNOWLEDGMENTS

This work was supported by the National Institutes of Health (1R01CA241194-01A1) grant to R.B. and F.J.S. All figures were created using BioRender.com.

REFERENCES

1. Nielsen PE, Egholm M, Berg RH, and Buchardt O (1991). Sequence-selective recognition of DNA by strand displacement with a thymine-substituted polyamide. Science 254, 1497–1500. 10.1126/science.1962210. [PubMed: 1962210]
2. Egli M, and Manoharan M (2019). Re-Engineering RNA Molecules into Therapeutic Agents. Acc. Chem. Res. 52, 1036–1047. 10.1021/acs.accounts.8b00650. [PubMed: 30912917]
3. Crooke ST, Baker BF, Crooke RM, and Liang X.-h. (2021). Antisense technology: an overview and prospectus. Nat. Rev. Drug Discov. 20, 427–453. 10.1038/s41573-021-00162-z. [PubMed: 33762737]
4. Egli M, and Manoharan M (2023). Chemistry, structure and function of approved oligonucleotide therapeutics. Nucleic Acids Res. 51, 2529–2573. 10.1093/nar/gkad067. [PubMed: 36881759]
5. Dragulescu-Andrasi A, Rapireddy S, Frezza BM, Gayathri C, Gil RR, and Ly DH (2006). A Simple γ-Backbone Modification Preorganizes Peptide Nucleic Acid into a Helical Structure. J. Am. Chem. Soc. 128, 10258–10267. 10.1021/ja0625576. [PubMed: 16881656]
6. Sahu B, Sacui I, Rapireddy S, Zanotti KJ, Bahal R, Armitage BA, and Ly DH (2011). Synthesis and Characterization of Conformationally Preorganized, (R)-Diethylene Glycol-Containing γ-Peptide

Nucleic Acids with Superior Hybridization Properties and Water Solubility. J. Org. Chem. 76, 5614–5627. 10.1021/jo200482d. [PubMed: 21619025]

7. Ricciardi AS, Bahal R, Farrelly JS, Quijano E, Bianchi AH, Luks VL, Putman R, Lopez-Giraldez F, Coskun S, Song E, et al. (2018). In utero nanoparticle delivery for site-specific genome editing. Nat. Commun. 9, 2481. 10.1038/s41467-018-04894-2. [PubMed: 29946143]
8. Bahal R, Ali McNeer N, Quijano E, Liu Y, Sulkowski P, Turchick A, Lu Y-C, Bhunia DC, Manna A, Greiner DL, et al. (2016). In vivo correction of anaemia in β-thalassemic mice by γPNA-mediated gene editing with nanoparticle delivery. Nat. Commun. 7, 13304. 10.1038/ncomms13304. [PubMed: 27782131]
9. Malik S, Pradeep SP, Kumar V, Xiao Y, Deng Y, Fan R, Vasquez JC, Singh V, and Bahal R (2024). Antitumor efficacy of a sequence-specific DNA-targeted γPNA-based c-Myc inhibitor. Cell Rep. Med. 5, 101354. 10.1016/j.xcrm.2023.101354. [PubMed: 38183981]
10. Dhuri K, Gaddam RR, Vikram A, Slack FJ, and Bahal R (2021). Therapeutic Potential of Chemically Modified, Synthetic, Triplex Peptide Nucleic Acid–Based Oncomir Inhibitors for Cancer Therapy. Cancer Res. 81, 5613–5624. 10.1158/0008-5472.Can-21-0736. [PubMed: 34548334]
11. Wang Y, Malik S, Suh H-W, Xiao Y, Deng Y, Fan R, Huttner A, Bindra RS, Singh V, Saltzman WM, and Bahal R (2023). Anti-seed PNAs targeting multiple oncomiRs for brain tumor therapy. Sci. Adv. 9, eabq7459. 10.1126/sciadv.abq7459. [PubMed: 36753549]
12. Wan WB, and Seth PP (2016). The Medicinal Chemistry of Therapeutic Oligonucleotides. J. Med. Chem. 59, 9645–9667. 10.1021/acs.jmedchem.6b00551. [PubMed: 27434100]
13. Henry S, Stecker K, Brooks D, Monteith D, Conklin B, and Bennett CF (2000). Chemically modified oligonucleotides exhibit decreased immune stimulation in mice. J. Pharmacol. Exp. Therapeut. 292, 468–479.
14. Østergaard ME, Kumar P, Nichols J, Watt A, Sharma PK, Nielsen P, and Seth PP (2015). Allele-Selective Inhibition of Mutant Huntingtin with 2-Thio- and C5-Triazolylphenyl-Deoxythymidine-Modified Antisense Oligonucleotides. Nucleic Acid Therapeut. 25, 266–274. 10.1089/nat.2015.0547.
15. Yoshida T, Morihiro K, Naito Y, Mikami A, Kasahara Y, Inoue T, and Obika S (2022). Identification of nucleobase chemical modifications that reduce the hepatotoxicity of gapmer antisense oligonucleotides. Nucleic Acids Res. 50, 7224–7234. 10.1093/nar/gkac562. [PubMed: 35801870]
16. Imaeda A, Tomoike F, Hayakawa M, Nakamoto K, Kimura Y, Abe N, and Abe H (2019). N(6)-methyl adenosine in siRNA evades immune response without reducing RNAi activity. Nucleos Nucleot. Nucleic Acids 38, 972–979. 10.1080/15257770.2019.1641205.
17. Lin K-Y, and Matteucci MD (1998). A Cytosine Analogue Capable of Clamp-Like Binding to a Guanine in Helical Nucleic Acids. J. Am. Chem. Soc. 120, 8531–8532. 10.1021/ja981286z.
18. Maier MA, Leeds JM, Balow G, Springer RH, Bharadwaj R, and Manoharan M (2002). Nuclease Resistance of Oligonucleotides Containing the Tricyclic Cytosine Analogues Phenoxazine and 9-(2-Aminoethoxy)-Phenoxazine (‘‘G-clamp’’) and Origins of Their Nuclease Resistance Properties. Biochemistry 41, 1323–1327. 10.1021/bi011725y. [PubMed: 11802733]
19. Rajeev KG, Maier MA, Lesnik EA, and Manoharan M (2002). High-Affinity Peptide Nucleic Acid Oligomers Containing Tricyclic Cytosine Analogues. Org. Lett. 4, 4395–4398. 10.1021/ol027026a. [PubMed: 12465896]
20. Koppelhus U, and Nielsen PE (2003). Cellular delivery of peptide nucleic acid (PNA). Adv. Drug Deliv. Rev. 55, 267–280. 10.1016/S0169-409X(02)00182-5. [PubMed: 12564980]
21. Nielsen PE (2005). Addressing the challenges of cellular delivery and bioavailability of peptide nucleic acids (PNA). Q. Rev. Biophys. 38, 345–350. 10.1017/S0033583506004148. [PubMed: 16600055]
22. Gupta A, Quijano E, Liu Y, Bahal R, Scanlon SE, Song E, Hsieh W-C, Braddock DE, Ly DH, Saltzman WM, and Glazer PM (2017). Anti-tumor Activity of miniPEG-γ-Modified PNAs to Inhibit MicroRNA-210 for Cancer Therapy. Mol. Ther. Nucleic Acids 9, 111–119. 10.1016/j.omtn.2017.09.001. [PubMed: 29246289]

23. Kumar V, Wahane A, Gupta A, Manautou JE, and Bahal R (2023). Multivalent Lactobionic Acid and N-Acetylgalactosamine-Conjugated Peptide Nucleic Acids for Efficient In Vivo Targeting of Hepatocytes. Adv. Healthcare Mater. 12, 2202859. 10.1002/adhm.202202859.
24. Ivanova GD, Arzumanov A, Abes R, Yin H, Wood MJA, Lebleu B, and Gait MJ (2008). Improved cell-penetrating peptide–PNA conjugates for splicing redirection in HeLa cells and exon skipping in mdx mouse muscle. Nucleic Acids Res. 36, 6418–6428. 10.1093/nar/gkn671. [PubMed: 18842625]
25. Cheng CJ, Bahal R, Babar IA, Pincus Z, Barrera F, Liu C, Svoronos A, Braddock DT, Glazer PM, Engelman DM, et al. (2015). MicroRNA silencing for cancer therapy targeted to the tumour microenvironment. Nature 518, 107–110. 10.1038/nature13905. [PubMed: 25409146]
26. Malik S, Slack FJ, and Bahal R (2020). Formulation of PLGA nanoparticles containing short cationic peptide nucleic acids. MethodsX 7, 101115. 10.1016/j.mex.2020.101115. [PubMed: 33145187]
27. Ahmadvand M, Eskandari M, Pashaiefar H, Yaghmaie M, Manoochehrabadi S, Khakpour G, Sheikhsaran F, and Montazer Zohour M (2018). Over expression of circulating miR-155 predicts prognosis in diffuse large B-cell lymphoma. Leuk. Res. 70, 45–48. 10.1016/j.leukres.2018.05.006. [PubMed: 29807272]
28. Anastasiadou E, Seto AG, Beatty X, Hermreck M, Gilles ME, Stroopinsky D, Pinter-Brown LC, Pestano L, Marchese C, Avigan D, et al. (2021). Cobomarsen, an Oligonucleotide Inhibitor of miR-155, Slows DLBCL Tumor Cell Growth In Vitro and In Vivo. Clin. Cancer Res. 27, 1139–1149. 10.1158/1078-0432.CCR-20-3139. [PubMed: 33208342]
29. Aloi MS, Prater KE, Sanchez REA, Beck A, Pathan JL, Davidson S, Wilson A, Keene CD, de la Iglesia H, Jayadev S, and Garden GA (2023). Microglia specific deletion of miR-155 in Alzheimer's disease mouse models reduces amyloid-beta pathology but causes hyperexcitability and seizures. J. Neuroinflammation 20, 60. 10.1186/s12974-023-02745-6. [PubMed: 36879321]
30. Beaurivage C, Champagne A, Tobelaim WS, Pomerleau V, Menendez A, and Saucier C (2016). SOCS1 in cancer: An oncogene and a tumor suppressor. Cytokine 82, 87–94. 10.1016/j.cyto.2016.01.005. [PubMed: 26811119]
31. Liu Y, Ao X, Ding W, Ponnusamy M, Wu W, Hao X, Yu W, Wang Y, Li P, and Wang J (2018). Critical role of FOXO3a in carcinogenesis. Mol. Cancer 17, 104. 10.1186/s12943-018-0856-3. [PubMed: 30045773]
32. Kim JH, Kim WS, and Park C (2012). Epstein-Barr virus latent membrane protein-1 protects B-cell lymphoma from rituximab-induced apoptosis through miR-155-mediated Akt activation and up-regulation of Mcl-1. Leuk. Lymphoma 53, 1586–1591. 10.3109/10428194.2012.659736. [PubMed: 22268450]
33. Kim S, Lee E, Jung J, Lee JW, Kim HJ, Kim J, Yoo HJ, Lee HJ, Chae SY, Jeon SM, et al. (2018). microRNA-155 positively regulates glucose metabolism via PIK3R1-FOXO3a-cMYC axis in breast cancer. Oncogene 37, 2982–2991. 10.1038/s41388-018-0124-4. [PubMed: 29527004]
34. Geng X, Sun YY, Fu JJ, Cao L, and Li Y (2020). Role of miR-155-5p expression and its involvement in apoptosis-related factors in thyroid follicular carcinoma. J. Clin. Pharm. Therapeut. 45, 660–665. 10.1111/jcpt.13175.
35. Dunleavy K (2021). Double-hit lymphoma: optimizing therapy. Hematology. Am. Soc. Hematol. Educ. Program 2021, 157–163. 10.1182/hematology.2021000247. [PubMed: 34889402]
36. DiSano JA, Huffnagle I, Gowda R, Spiegelman VS, Robertson GP, and Pameijer CR (2019). Loss of miR-155 upregulates WEE1 in metastatic melanoma. Melanoma Res. 29, 216–219. 10.1097/CMR.0000000000000545. [PubMed: 30499870]
37. Manganelli F, Fabrizi GM, Luigetti M, Mandich P, Mazzeo A, and Pareyson D (2022). Hereditary transthyretin amyloidosis overview. Neurol. Sci. 43, 595–604. 10.1007/s10072-020-04889-2. [PubMed: 33188616]
38. Adams D, Algalarrondo V, and Echaniz-Laguna A (2023). Hereditary transthyretin amyloidosis in the era of RNA interference, antisense oligonucleotide, and CRISPR-Cas9 treatments. Blood 142, 1600–1612. 10.1182/blood.2023019884. [PubMed: 37624911]

39. Bentin T, Larsen HJ, and Nielsen PE (2003). Combined triplex/duplex invasion of double-stranded DNA by “tail-clamp” peptide nucleic acid. Biochemistry 42, 13987–13995. 10.1021/bi0351918. [PubMed: 14636067]
40. Suparpprom C, and Vilaivan T (2022). Perspectives on conformationally constrained peptide nucleic acid (PNA): insights into the structural design, properties and applications. RSC Chem. Biol. 3, 648–697. 10.1039/d2cb00017b.
41. Dragulescu-Andrasi A, Zhou P, He G, and Ly DH (2005). Cell-permeable GPNA with appropriate backbone stereochemistry and spacing binds sequence-specifically to RNA. Chem. Commun. 60, 244–246. 10.1039/b412522c.
42. Sugiyama T, Imamura Y, Demizu Y, Kurihara M, Takano M, and Kittaka A (2011). β-PNA: peptide nucleic acid (PNA) with a chiral center at the β-position of the PNA backbone. Bioorg. Med. Chem. Lett. 21, 7317–7320. 10.1016/j.bmcl.2011.10.017. [PubMed: 22050888]
43. Pradeep SP, Malik S, Slack FJ, and Bahal R (2023). Unlocking the potential of chemically modified peptide nucleic acids for RNA-based therapeutics. RNA 29, 434–445. 10.1261/rna.079498.122. [PubMed: 36653113]
44. Ausín C, Ortega JA, Robles J, Grandas A, and Pedroso E (2002). Synthesis of amino- and guanidino-G-clamp PNA monomers. Org. Lett. 4, 4073–4075. 10.1021/ol026815p. [PubMed: 12423089]
45. Flanagan WM, Wolf JJ, Olson P, Grant D, Lin KY, Wagner RW, and Matteucci MD (1999). A cytosine analog that confers enhanced potency to antisense oligonucleotides. Proc. Natl. Acad. Sci. USA 96, 3513–3518. 10.1073/pnas.96.7.3513. [PubMed: 10097067]
46. Chenna V, Rapireddy S, Sahu B, Ausin C, Pedroso E, and Ly DH (2008). A simple cytosine to G-clamp nucleobase substitution enables chiral gamma-PNAs to invade mixed-sequence double-helical B-form DNA. Chembiochem 9, 2388–2391. 10.1002/cbic.200800441. [PubMed: 18816545]
47. Rapireddy S, Bahal R, and Ly DH (2011). Strand invasion of mixed-sequence, double-helical B-DNA by gamma-peptide nucleic acids containing G-clamp nucleobases under physiological conditions. Biochemistry 50, 3913–3918. 10.1021/bi2002554. [PubMed: 21476606]
48. Wahba AS, Azizi F, Deleavey GF, Brown C, Robert F, Carrier M, Kalota A, Gewirtz AM, Pelletier J, Hudson RHE, and Damha MJ (2011). Phenylpyrrolocytosine as an Unobtrusive Base Modification for Monitoring Activity and Cellular Trafficking of siRNA. ACS Chem. Biol. 6, 912–919. 10.1021/cb200070k. [PubMed: 21667942]
49. Hu J, Matsui M, and Corey DR (2009). Allele-selective inhibition of mutant huntingtin by peptide nucleic acid-peptide conjugates, locked nucleic acid, and small interfering RNA. Ann. N. Y. Acad. Sci. 1175, 24–31. 10.1111/j.1749-6632.2009.04975.x. [PubMed: 19796074]
50. Wojciechowski F, and Hudson RH (2009). Peptide nucleic acid containing a meta-substituted phenylpyrrolocytosine exhibits a fluorescence response and increased binding affinity toward RNA. Org. Lett. 11, 4878–4881. 10.1021/ol9019474. [PubMed: 19788268]
51. Ryan CA, Brodyagin N, Lok J, and Rozners E (2021). The 2-Aminopyridine Nucleobase Improves Triple-Helical Recognition of RNA and DNA When Used Instead of Pseudoisocytosine in Peptide Nucleic Acids. Biochemistry 60, 1919–1925. 10.1021/acs.biochem.1c00275. [PubMed: 34097400]
52. Kim K, Kim HH, Lee CH, Kim S, Cheon GJ, Kang KW, Chung JK, and Youn H (2020). Therapeutic efficacy of modified anti-miR21 in metastatic prostate cancer. Biochem. Biophys. Res. Commun. 529, 707–713. 10.1016/j.bbrc.2020.05.215. [PubMed: 32736696]
53. Malik S, Lim J, Slack FJ, Braddock DT, and Bahal R (2020). Next generation miRNA inhibition using short anti-seed PNAs encapsulated in PLGA nanoparticles. J. Contr. Release 327, 406–419. 10.1016/j.jconrel.2020.08.026.
54. Ahangari F, Price NL, Malik S, Chioccioli M, Barnthaler T, Adams TS, Kim J, Pradeep SP, Ding S, Cosmos C Jr., et al. (2023). microRNA-33 deficiency in macrophages enhances autophagy, improves mitochondrial homeostasis, and protects against lung fibrosis. JCI Insight 8, e158100. 10.1172/jci.insight.158100. [PubMed: 36626225]
55. Zhang X, Rotllan N, Canfran-Duque A, Sun J, Toczek J, Moshnikova A, Malik S, Price NL, Araldi E, Zhong W, et al. (2022). Targeted Suppression of miRNA-33 Using pHLIP Improves

Atherosclerosis Regression. Circ. Res. 131, 77–90. 10.1161/CIRCRESAHA.121.320296. [PubMed: 35534923]

56. Dhuri K, Vyas RN, Blumenfeld L, Verma R, and Bahal R (2021). Nanoparticle Delivered Anti-miR-141-3p for Stroke Therapy. Cells 10, 1011. 10.3390/cells10051011. [PubMed: 33922958]
57. Fabani MM, and Gait MJ (2008). miR-122 targeting with LNA/2'-O-methyl oligonucleotide mixmers, peptide nucleic acids (PNA), and PNA-peptide conjugates. RNA 14, 336–346. 10.1261/rna.844108. [PubMed: 18073344]
58. Papi C, Gasparello J, Zurlo M, Manicardi A, Corradini R, Cabrini G, Gambari R, and Finotti A (2022). Combined Treatment of Bronchial Epithelial Calu-3 Cells with Peptide Nucleic Acids Targeting miR-145-5p and miR-101-3p: Synergistic Enhancement of the Expression of the Cystic Fibrosis Transmembrane Conductance Regulator (CFTR) Gene. Int. J. Mol. Sci. 23, 9348. 10.3390/ijms23169348. [PubMed: 36012615]
59. Ghavami M, Shiraishi T, and Nielsen PE (2019). Cooperative Cellular Uptake and Activity of Octaarginine Antisense Peptide Nucleic acid (PNA) Conjugates. Biomolecules 9, 554. 10.3390/biom9100554. [PubMed: 31581514]
60. Nam SH, Park J, and Koo H (2023). Recent advances in selective and targeted drug/gene delivery systems using cell-penetrating peptides. Arch Pharm. Res. (Seoul) 46, 18–34. 10.1007/s12272-022-01425-y.
61. Fröhlich E (2012). The role of surface charge in cellular uptake and cytotoxicity of medical nanoparticles. Int. J. Nanomed. 7, 5577–5591. 10.2147/IJN.S36111.
62. Kedmi R, Ben-Arie N, and Peer D (2010). The systemic toxicity of positively charged lipid nanoparticles and the role of Toll-like receptor 4 in immune activation. Biomaterials 31, 6867–6875. 10.1016/j.biomaterials.2010.05.027. [PubMed: 20541799]
63. Poli L, Labella B, Cotti Piccinelli S, Caria F, Risi B, Damioli S, Padovani A, and Filosto M (2023). Hereditary transthyretin amyloidosis: a comprehensive review with a focus on peripheral neuropathy. Front. Neurol. 14, 1242815. 10.3389/fneur.2023.1242815. [PubMed: 37869146]
64. Rowczenio DM, Noor I, Gillmore JD, Lachmann HJ, Whelan C, Hawkins PN, Obici L, Westermark P, Grateau G, and Wechalekar AD (2014). Online registry for mutations in hereditary amyloidosis including nomenclature recommendations. Hum. Mutat. 35, E2403–E2412. 10.1002/humu.22619. [PubMed: 25044787]
65. Delgado E, Bahal R, Yang J, Lee JM, Ly DH, and Monga SP (2013). β-Catenin knockdown in liver tumor cells by a cell permeable gamma guanidine-based peptide nucleic acid. Curr. Cancer Drug Targets 13, 867–878. 10.2174/15680096113139990081. [PubMed: 23822752]
66. Butler JS, Chan A, Costelha S, Fishman S, Willoughby JL, Borland TD, Milstein S, Foster DJ, Goncalves P, Chen Q, et al. (2016). Preclinical evaluation of RNAi as a treatment for transthyretin-mediated amyloidosis. Amyloid 23, 109–118. 10.3109/13506129.2016.1160882. [PubMed: 27033334]
67. Hutvagner G, and Zamore PD (2002). A microRNA in a multiple-turnover RNAi enzyme complex. Science 297, 2056–2060. 10.1126/science.1073827. [PubMed: 12154197]
68. Whitehead KA, Langer R, and Anderson DG (2009). Knocking down barriers: advances in siRNA delivery. Nat. Rev. Drug Discov. 8, 129–138. 10.1038/nrd2742. [PubMed: 19180106]
69. Adams D, Gonzalez-Duarte A, O'Riordan WD, Yang CC, Ueda M, Kristen AV, Tournev I, Schmidt HH, Coelho T, Berk JL, et al. (2018). Patisiran, an RNAi Therapeutic, for Hereditary Transthyretin Amyloidosis. N. Engl. J. Med. 379, 11–21. 10.1056/NEJMoa1716153. [PubMed: 29972753]
70. Ibrahim RB, Liu YT, Yeh SY, and Tsai JW (2019). Contributions of Animal Models to the Mechanisms and Therapies of Transthyretin Amyloidosis. Front. Physiol. 10, 338. 10.3389/fphys.2019.00338. [PubMed: 31001136]
71. Ammala C, Drury WJ 3rd, Knerr L, Ahlstedt I, Stillemark-Billton P, Wennberg-Huldt C, Andersson EM, Valeur E, Jansson-Lofmark R, Janzen D, et al. (2018). Targeted delivery of antisense oligonucleotides to pancreatic beta-cells. Sci. Adv. 4, eaat3386. 10.1126/sciadv.aat3386. [PubMed: 30345352]
72. Yan W, Li Y, Xie S, Tao WA, Hu J, Liu H, Zhang G, Liu F, Nie Y, Chen X, et al. (2024). Chondrocyte-Targeted Delivery System of Sortase A-Engineered Extracellular Vesicles

Silencing MMP13 for Osteoarthritis Therapy. Adv. Healthcare Mater. 13, e2303510. 10.1002/adhm.202303510.

73. Taghdisi SM, Danesh NM, Lavaee P, Emrani AS, Hassanabad KY, Ramezani M, and Abnous K (2016). Double targeting, controlled release and reversible delivery of daunorubicin to cancer cells by polyvalent aptamers-modified gold nanoparticles. Mater. Sci. Eng, C 61, 753–761. 10.1016/j.msec.2016.01.009.
74. Zhang Y, Roccaro AM, Rombaoa C, Flores L, Obad S, Fernandes SM, Sacco A, Liu Y, Ngo H, Quang P, et al. (2012). LNA-mediated anti-miR-155 silencing in low-grade B-cell lymphomas. Blood 120, 1678–1686. 10.1182/blood-2012-02-410647. [PubMed: 22797699]
75. Willoughby JLS, Chan A, Sehgal A, Butler JS, Nair JK, Racie T, Shulga-Morskaya S, Nguyen T, Qian K, Yucius K, et al. (2018). Evaluation of GalNAc-siRNA Conjugate Activity in Pre-clinical Animal Models with Reduced Asialoglycoprotein Receptor Expression. Mol. Ther. 26, 105–114. 10.1016/j.ymthe.2017.08.019. [PubMed: 28988716]
76. Witten L, and Slack FJ (2020). miR-155 as a novel clinical target for hematological malignancies. Carcinogenesis 41, 2–7. 10.1093/carcin/bgz183. [PubMed: 31711135]
77. McGinnis S, and Madden TL (2004). BLAST: at the core of a powerful and diverse set of sequence analysis tools. Nucleic Acids Res. 32, W20–W25. 10.1093/nar/gkh435. [PubMed: 15215342]
78. Liu Z, Venkatesh SS, and Maley CC (2008). Sequence space coverage, entropy of genomes and the potential to detect non-human DNA in human samples. BMC Genom. 9, 509. 10.1186/1471-2164-9-509.
79. Koppelhus U, and Nielsen PE (2003). Cellular delivery of peptide nucleic acid (PNA). Adv. Drug Deliv. Rev. 55, 267–280. 10.1016/s0169-409x(02)00182-5. [PubMed: 12564980]
80. Wahane A, Malik S, Shih K-C, Gaddam RR, Chen C, Liu Y, Nieh M-P, Vikram A, and Bahal R (2021). Dual-Modality Poly-l-histidine Nanoparticles to Deliver Peptide Nucleic Acids and Paclitaxel for In Vivo Cancer Therapy. ACS Appl. Mater. Interfaces 13, 45244–45258. 10.1021/acsami.1c11981. [PubMed: 34524806]
81. Deng Y, Saucier-Sawyer JK, Hoimes CJ, Zhang J, Seo YE, Andrejecsk JW, and Saltzman WM (2014). The effect of hyperbranched polyglycerol coatings on drug delivery using degradable polymer nanoparticles. Biomaterials 35, 6595–6602. 10.1016/j.biomaterials.2014.04.038. [PubMed: 24816286]

Highlights

- Clamp-G nucleobase enhances the binding affinity of PNA to target miRNA and mRNA
- Clamp-G PNA inhibits oncomiR-155 in multiple lymphoma cell lines
- Clamp-G PNA efficiently knocks down TTR mRNA
- Clamp-G PNAs are effective RNA inhibitors for other antisense therapies

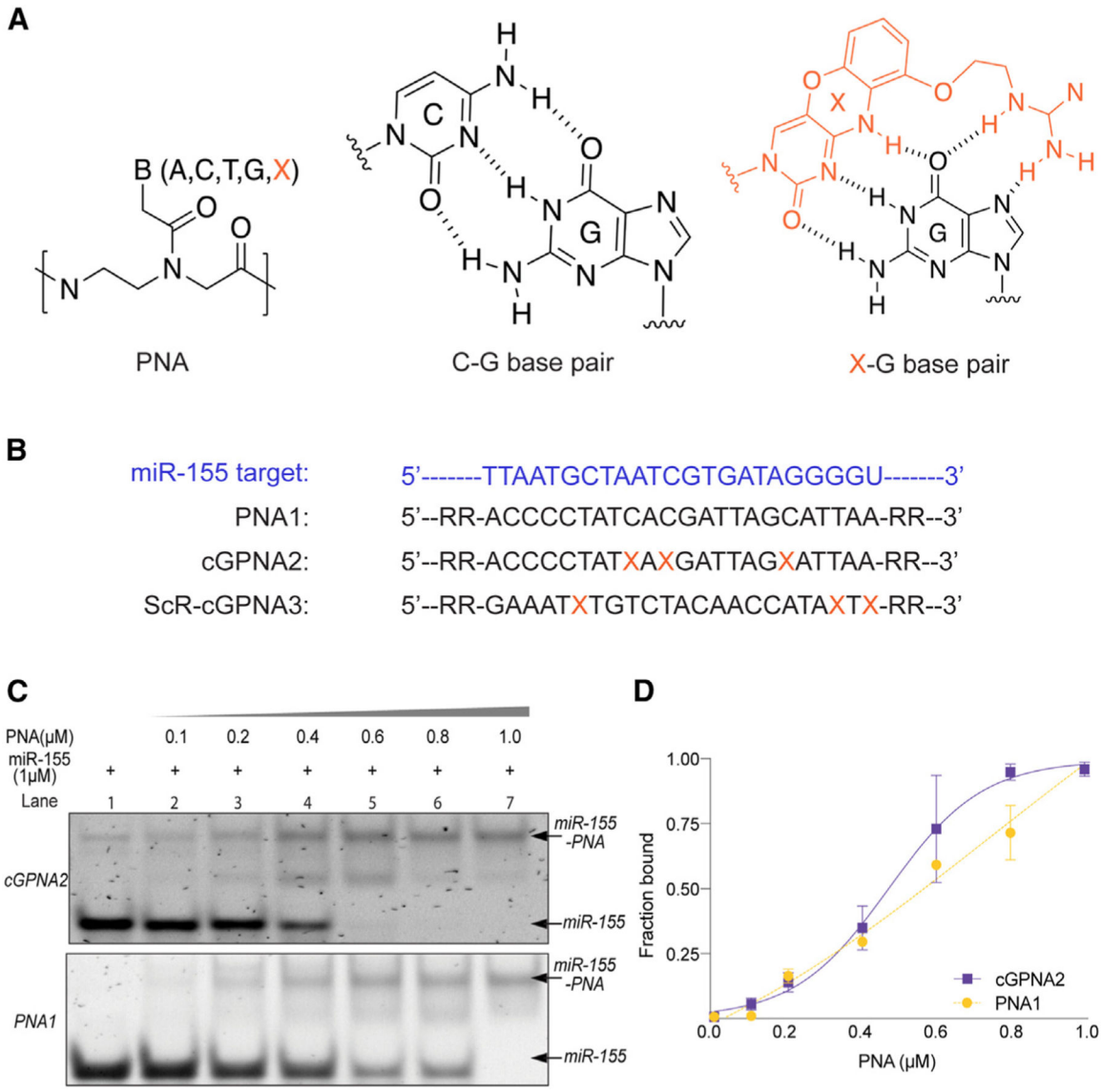

Figure 1. Design of PNA oligomers and gel shift binding assay

(A) Chemical structure of PNA where B signifies adenine (A), guanine (G), cytosine (C), thymine (T), and clamp-G (X). Chemical structures of C-G and X-G base pairs. C-G forms three H-bonds and X-G forms five H-bonds.

(B) The sequence of oncomiR-155 and PNAs used in the study. PNA1 and clamp-G PNA2 (cGPNA2) are designed to bind to miR-155. Scramble cGPNA3 (ScR-cGPNA3) was synthesized as a control. The PNAs have two arginine (R) residues on the N (5′) and C (3′) terminals. Orange, X monomer.

(C) Dose-dependent gel shift binding assay of target miR-155 (1 μM) with PNA1 and cGPNA2 at indicated concentrations. The samples were prepared in physiological buffer (2 mmol/L $MgCl_2$, 150 mmol/L KCl, and 10 mmol/L NaPi) and incubated for 16 h at physiological temperature (37°C), followed by PAGE separation and visualization of bands by SYBR Gold staining.

(D) Graph representing the quantification of the bound fraction of PNA1 and cGPNA2. The data are represented as mean ± SEM ($n = 3$).

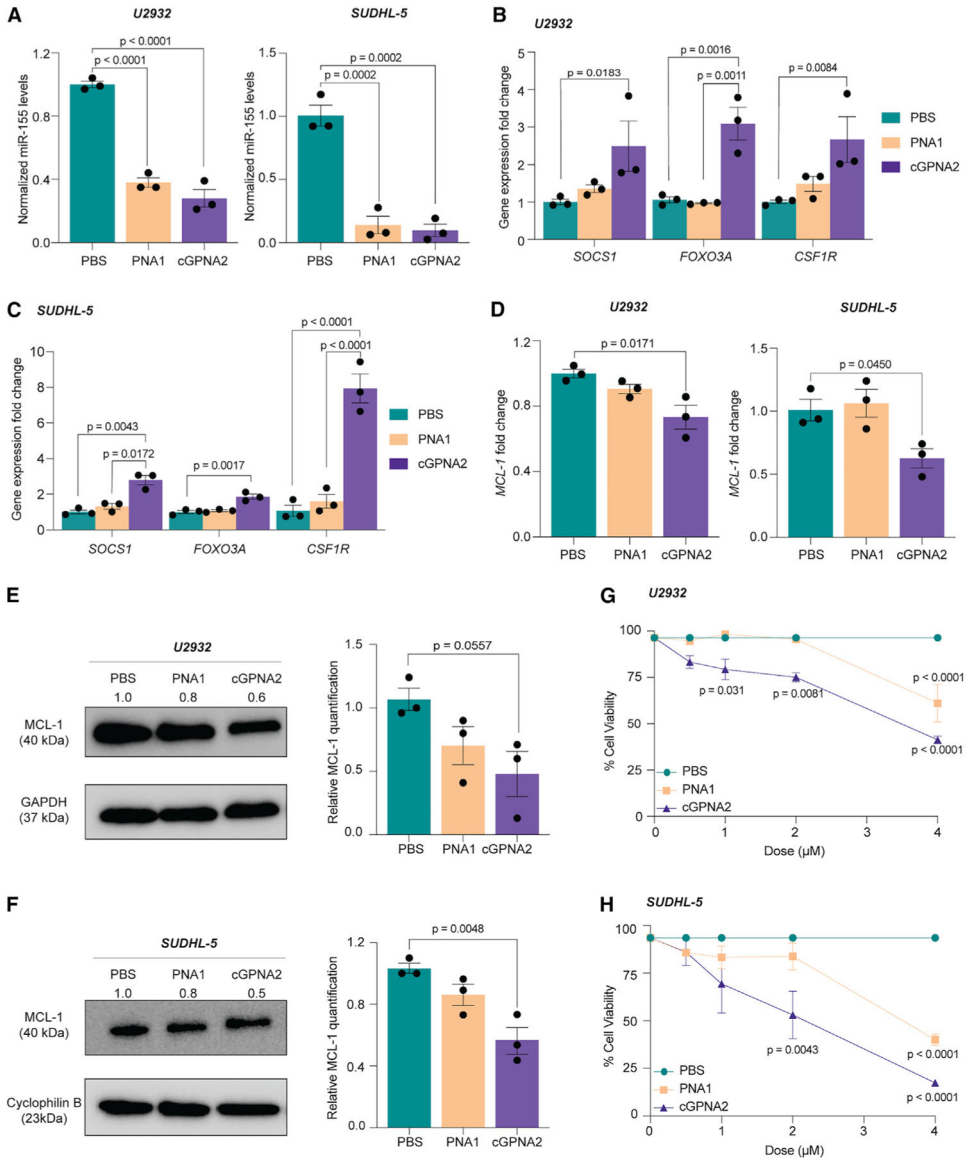

Figure 2. Antisense activity of clamp-G PNA in lymphoma cells

(A) Relative fold change in the levels of miR-155 after treatment of U2932 and SUDHL-5 lymphoma cells with PBS (control), PNA1, and cGPNA2. Data were normalized against *U6* endogenous control.

(B and C) Gene expression of miR-155 downstream target genes (*SOCS1*, *FOXO3A*, *CSF1R*) in (B) U2932 and (C) SUDHL-5 cell lines after treatment with PBS (control), PNA1, and cGPNA2. Data were normalized against *GAPDH* endogenous control.

(D) Relative fold change in the levels *MCL-1* oncogene in U2932 and SUDHL-5 cells treated with PBS (control), PNA1, and cGPNA2. (E and F) Representative western blot of MCL-1 protein fold change in U2932 and SUDHL-5 cells (left) after 48-h treatment with PBS (control), PNA1, and cGPNA2. The graphs (right) represent the quantification of MCL-1 protein fold change in U2932 and SUDHL-5 cells after indicated treatment relative to PBS.

(A–E) U2932 and SUDHL-5 cells were treated with indicated PNAs at 4 μM dose for 48 h. (G and H) The percentage cell viability of U2932 (top) and SUDHL-5 (bottom) treated with PBS, PNA1, and cGPNA2 at increasing concentrations (0.5, 1, 2, 4 μM) for 48 h. (A–H) The results are represented as mean ± SEM ($n = 3$ biological replicates). An unpaired two-sample t test was used for statistical analysis.

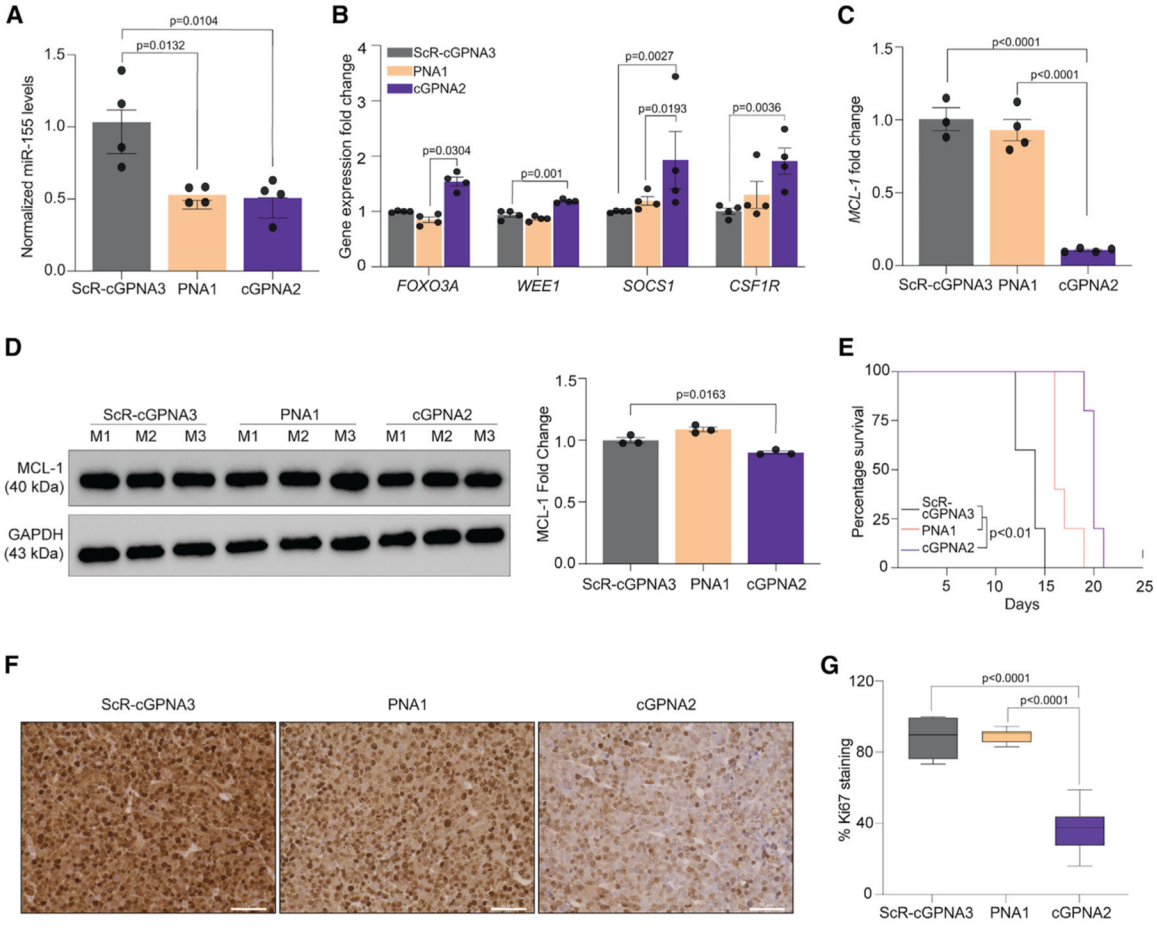

Figure 3. Evaluating the efficacy of anti-miR-155 therapy in the U2932 xenograft mouse model

(A) Relative fold change in the levels of miR-155 in ScR-cGPNA3-, PNA1-, and cGPNA2-treated U2932 tumors. Data were normalized against *U6* endogenous control.

(B) Gene expression of miR-155 downstream target genes (*FOXO3A*, *WEE1*, *SOCS1*, and *CSF1R*) in ScR-cGPNA3-, PNA-1-, and cGPNA2-treated U2932 tumors. Data were normalized against *GAPDH* endogenous control.

(C) Relative fold change in the mRNA levels of miR-155 downstream gene *MCL-1* oncogene in ScR-cGPNA3, PNA1, and cGPNA2.

(D) Representative western blot of MCL-1 protein fold change (left) in ScR-cGPNA3, PNA1, and cGPNA2. The graphs (right) represent the quantification of MCL-1 protein fold change after indicated treatment relative to ScR-cGPNA3. (A–D) Mice were treated with 5 mg/kg, intratumorally for 48 h. Graph shows mean ± SEM ($n = 6$) and p value is from two-way ANOVA.

(E) Survival curve for tumors treated with ScR-cGPNA3, PNA1, and cGPNA2. The survival endpoint was a tumor volume of 2,000 mm^2 and plotted against the number of days ($n =$ 6 mice in each treatment group). Log rank Mantle-Cox test was performed for statistical significance of percentage survival.

(F) Representative immunohistochemistry images Ki67 staining in ScR-cGPNA3, PNA1, and cGPNA2 collected at the end of survival study. Scale bar, 50 μm.

(G) Box-plot representing the Ki67 quantification in tumor sections from indicated groups. The results are plotted to include all data points, and $n > 4$ images were quantified per tumor section ScR-cGPNA3 ($n = 2$), PNA1 ($n = 2$), and cGPNA-2 ($n = 2$). An unpaired two-sample t test was used for statistical analysis.

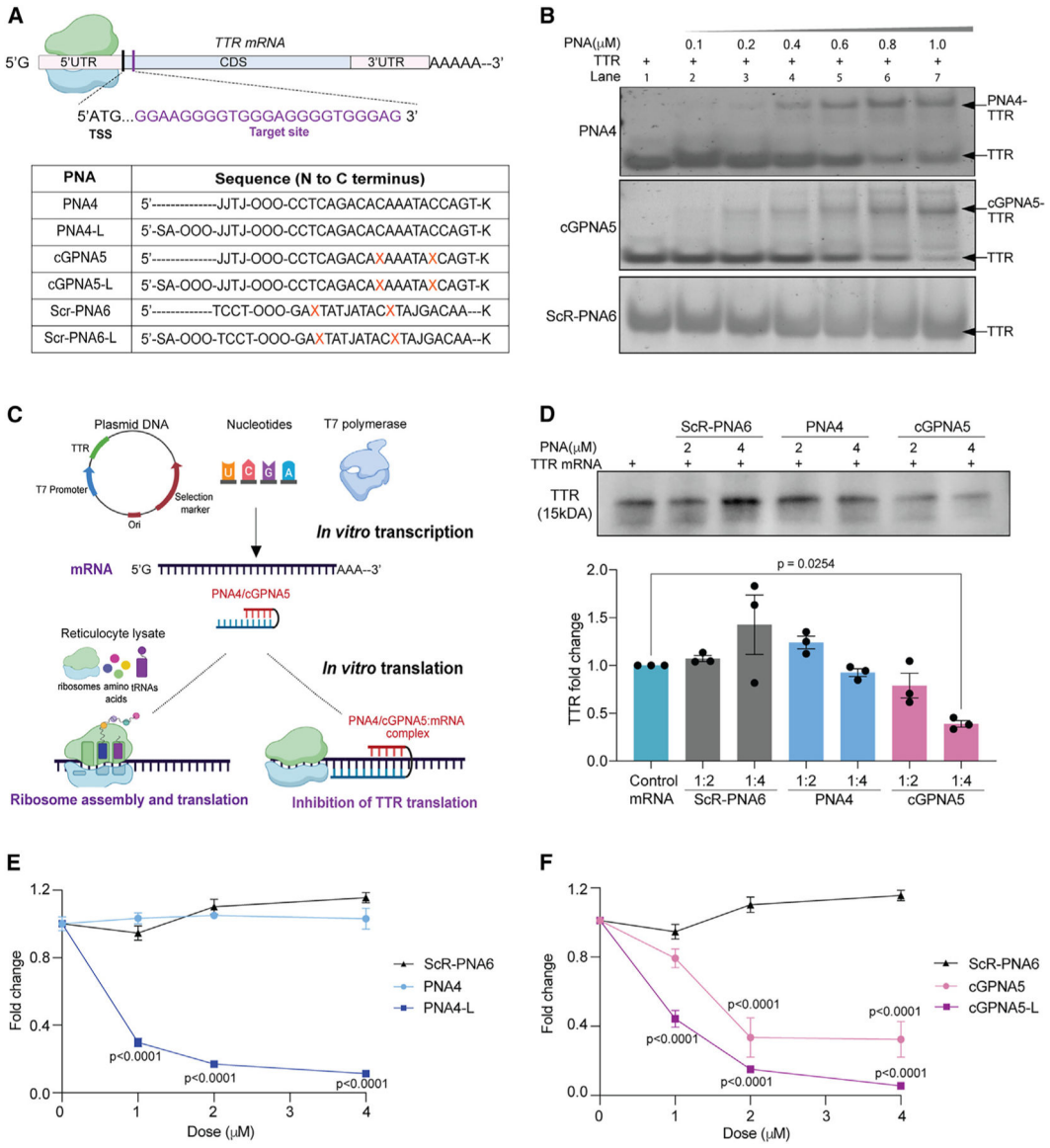

PNA	Sequence (N to C terminus)
PNA4	5'----------JJTJ-OOO-CCTCAGACACAAATACCAGT-K
PNA4-L	5'-SA-OOO-JJTJ-OOO-CCTCAGACACAAATACCAGT-K
cGPNA5	5'----------JJTJ-OOO-CCTCAGACAXAAATAXCAGT-K
cGPNA5-L	5'-SA-OOO-JJTJ-OOO-CCTCAGACAXAAATAXCAGT-K
Scr-PNA6	5'----------TCCT-OOO-GAXTATJATACXTAJGACAA---K
Scr-PNA6-L	5'-SA-OOO-TCCT-OOO-GAXTATJATACXTAJGACAA--K

Figure 4. Evaluating the ability of clamp-G PNA to bind and inhibit TTR mRNA

(A) Graphic representation of target site on TTR mRNA. The table contains PNA oligomer sequences to the TTR target site. PNA4-LBA, cGPNA5-L, and ScR-PNA6-L contain succinic acid (SA) at the 5′ end (N terminus) for conjugation with LBA ligand. Lysine (K) was added at the 3′ end (C terminus) of the PNA, and OOO represents the trioxo-miniPEG linker.

(B) Dose-dependent gel shift assay of TTR target with PNA4, cGPNA5, and ScR-PNA6 at indicated concentration. Samples were incubated in physiological buffer (2 mmol/L $MgCl_2$, 150 mmol/L KCl, and 10 mmol/L NaPi) for 16 h at 37°C, followed by PAGE separation.

(C) Schematic representation of PNA inhibiting translation initiation of TTR mRNA. Plasmid containing TTR coding region, nucleotides, and T7 polymerase were used to make TTR mRNA via *in vitro* transcription. TTR mRNA was incubated with different concentrations of PNA, and *in vitro* translation was performed using reticulocyte lysate.

(D) Representative western blot analysis (top) of TTR protein after PNA and TTR mRNA incubation in reticulocyte lysate. The graph (bottom) represents the quantification of TTR protein fold change relative to the control. ImageJ was used for quantification, the graph shows mean ± SEM ($n = 3$), and the p value is from two-way ANOVA.
(E) Fold change in *TTR* mRNA levels in HepG2 cells treated with indicated doses of PNA4 and PNA4-L in comparison to ScR-PNA6.
(F) Relative change in *TTR* mRNA levels in HepG2 cells treated with indicated doses of cGPNA5 and cGPNA5-L doses in comparison to ScR-PNA6. Graph shows mean ± SEM ($n = 3$) and p value is from two-way ANOVA.

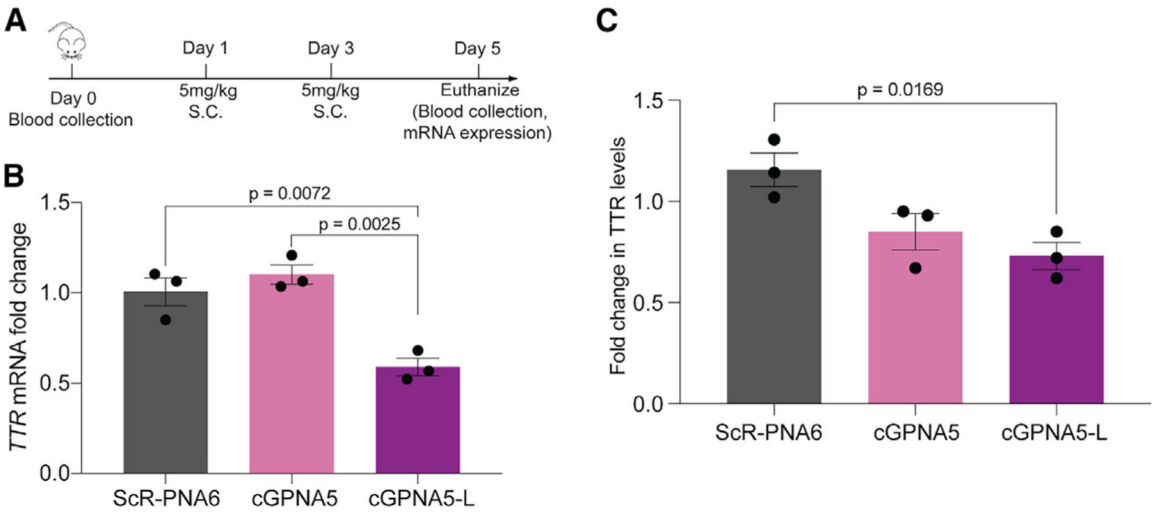

Figure 5. Efficacy of TTR clamp-G PNAs activity *in vivo*

(A) Workflow representing short-term evaluation of cGPNA5 in C56BL/6J mice post subcutaneous administration at 5 mg/kg.

(B) Relative fold change in the levels of TTR in livers of ScR-cGPNA6-L, cGPNA5, and cGPNA5-L. Graph shows mean ± SEM ($n = 3$) and p value is from two-way ANOVA.

(C) Quantification of relative fold change in plasma TTR protein levels of ScR-cGPNA6-L, cGPNA5, and cGPNA5-L by ELISA. Graph shows mean ± SEM ($n = 3$) and p value is from two-way ANOVA.